Influence of the Shape of Copper Powder Particles on the Crystal Structure and Some Decisive Characteristics of the Metal Powders

Ljiljana Avramović [1], Vesna M. Maksimović [2], Zvezdana Baščarević [3], Nenad Ignjatović [4], Mile Bugarin [1], Radmila Marković [1] and Nebojša D. Nikolić [5],*

1. Mining and Metallurgy Institute, Center for Technologies Development in Metallurgy, Zeleni bulevar 35, 19 210 Bor, Serbia; ljiljana.avramovic@irmbor.co.rs (L.A.); mile.bugarin@irmbor.co.rs (M.B.); radmila.markovic@irmbor.co.rs (R.M.)
2. Vinča Institute of Nuclear Sciences, Department of Materials Science, University of Belgrade, 11 000 Belgrade, Serbia; vesnam@vin.bg.ac.rs
3. Institute for Multidisciplinary Research, University of Belgrade, Kneza Višeslava 1a, 11 000 Belgrade, Serbia; zvezdana@imsi.bg.ac.rs
4. Institute of Technical Sciences of the Serbian Academy of Science and Arts, Knez Mihailova 35/IV, 11 000 Belgrade, Serbia; nenad.ignjatovic@itn.sanu.ac.rs
5. Institute of Chemistry, Technology and Metallurgy-Department of Electrochemistry, University of Belgrade, Njegoševa 12, 11 000 Belgrade, Serbia
* Correspondence: nnikolic@ihtm.bg.ac.rs; Tel.: +381-11-337-0390

Abstract: Three different forms of Cu powder particles obtained by either galvanostatic electrolysis or a non-electrolytic method were analyzed by a scanning electron microscope (SEM), X-ray diffraction (XRD) and particle size distribution (PSD). Electrolytic procedures were performed under different hydrogen evolution conditions, leading to the formation of either 3D branched dendrites or disperse cauliflower-like particles. The third type of particles were compact agglomerates of the Cu grains, whose structural characteristics indicated that they were formed by a non-electrolytic method. Unlike the sharp tips that characterize the usual form of Cu dendrites, the ends of both the trunk and branches were globules in the formed dendrites, indicating that a novel type of Cu dendrites was formed in this investigation. Although the macro structures of the particles were extremely varied, they had very similar micro structures because they were constructed by spherical grains. The Cu crystallites were randomly oriented in the dendrites and compact agglomerates of the Cu grains, while the disperse cauliflower-like particles showed (220) and (311) preferred orientation. This indicates that the applied current density affects not only the morphology of the particles, but also their crystal structure. The best performance, defined by the largest specific surface area and the smallest particle size, was by the galvanostatically produced powder consisting of disperse cauliflower-like particles.

Keywords: copper; powder; electrolysis; hydrogen; SEM; XRD; PSD

1. Introduction

Copper powders have found a wide industrial application for a very long time [1]. Cu in a powder form is often used in the electrical and electronic industries due to its excellent electrical and thermal characteristics. The self-lubricating bearing is probably the most common application of Cu powder and about 70% of the total Cu powder production in a granular form is used for that purpose. This application takes advantage of the ability to produce a component with controlled interconnected and surface-connected porosity. Copper powders are also used in such nonstructural applications as

brazing, cold soldering, and mechanical plating, as well as for medals and medallions, metal-plastic decorative products and a variety of chemical and medical purposes.

The Cu powder production methods can be divided into electrolytic and non-electrolytic (or chemical) methods. Processes such as ultrasonic spray pyrolysis [2], solvothermal synthesis [3], cementation [4], chemical reduction methods [5–8], the high-energy electrical explosion method [9], atomization [10], pyrolysis [11], polyol processes [12–14], hydrometallurgy [15], etc. belong to the group of non-electrochemical or chemical processes of synthesis. The chemical reduction method is often referred to as electroless deposition [15,16]. Various reducing agents, such as ascorbic acid [5,8,16], hydrazine hydrate [7], sodium borohydride [6], and formaldehyde [15], are used in the chemical reduction processes. Copper, in the form of nanoparticles, can be synthesized in ethylene glycol (EG) using copper sulphate as a precursor, and vanadium sulfate as an atypical reductant [17]. Metal nanoparticles can also be obtained by biosynthesis processes using the microorganisms, which has clear advantages compared to chemical synthesis methods [18]. The biosynthesis processes are environmentally friendly, no toxic chemicals or reagents are needed for these processes, and it is possible to synthesize particles that cannot be obtained using chemical synthesis methods.

Aside from the above-mentioned methods of synthesis, electrolysis is often used for Cu powder synthesis. The advantage of this method of synthesis can primarily be attributed to the fact that the shape and size of particles can be easily regulated by the choice of electrolysis regime and parameters [19]. The regimes, both constant (potentiostatic [20] and galvanostatic [21–23]) and periodically changing [19,24–26], are used for the Cu synthesis in powder form. The electrolysis parameters that affect the final shape of the particles, are: the type and composition of electrolytes, presence of additives, temperature, type of cathode, electrolysis time, etc. [19,21,25,27–30]. Special attention has been dedicated to the effect of the hydrogen evolution reaction as the parallel reaction to Cu electrolysis in the production range of Cu powder [20,24].

The shape of Cu powder particles is related to their synthesis method. The four various forms of Cu particles can be identified as: almost ideal micro spheres, irregular rough particles, disperse cauliflower-like particles and dendrites. Dendrites are the most commonly observed shape of particles and they can be obtained by both electrolysis and some chemical methods such as the galvanic replacement reaction method [31]. The very disperse cauliflower-like particles are formed by the electrolysis in conditions of strong hydrogen evolution as the parallel reaction [19,20]. Irregular particles are obtained by water atomization [32] while spherical particles are obtained by the gas-atomizing process [32]. Aggregates of non-uniform irregular particles are obtained by the polyol process [12]. Almost ideal Cu spheres can be also obtained by the polyol process [12]. Polyhedral, non-agglomerated monodispersed particles are obtained using ascorbic acid as the reducing agent [4]. The non-agglomerated almost spherical particles are obtained by ultrasonic spray pyrolysis [2].

Recently, a strong correlation between the morphologies of silver powder particles and their crystal structure was found [33,34]. Here, this type of investigation has been continued with the aim of establishing the existence of the same correlation for Cu powders. For this reason, the three completely various morphologies of Cu powder particles were analyzed and correlated with their crystal structure. Two of them are obtained by electrolysis under completely different conditions, without and with vigorous hydrogen evolution. The third type was commercially supplied, and on the basis of morphological characteristics, it is clear that it was obtained by some non-electrochemical method. In order to examine the effect of the shape of particles on the decisive characteristics that define the behavior of the powders as a collection of particles, the specific surface area (SSA) and particle size distribution (PSD) were also analyzed.

2. Materials and Methods

Electrolyte, formed by dissolution of 0.10 mol·dm^{-3} CuSO$_4$ in 0.50 mol·dm^{-3} H$_2$SO$_4$, was used for the electrolytic production of Cu powders. Cu powder was galvanostatically produced at the current densities of 14.4 and 384 mA·cm^{-2}. Hereinafter, these powders are denoted as Cu(14.4) for

powder produced at 14.4 mA·cm^{-2} and Cu(384) for powder produced at 384 mA·cm^{-2}. Electrolysis was carried out at a temperature of 21.0 ± 0.5 °C in an open cell of cylindrical shape. The cylindrical Cu wire of the overall surface area 0.50 cm^2 was used as the working electrode. The counter electrode was Cu foil. Figure 1 shows a configuration of electrodes in the cell. The ultra-pure water and p.a. reagents (CuSO$_4 \times$ 5H$_2$O, H$_2$SO$_4$) were used for electrolyte preparation for the Cu powder synthesis. Powder was produced with the electricity amount of 10 mA·h·cm^{-2}, and removed from the electrode surface after this amount of electricity was reached.

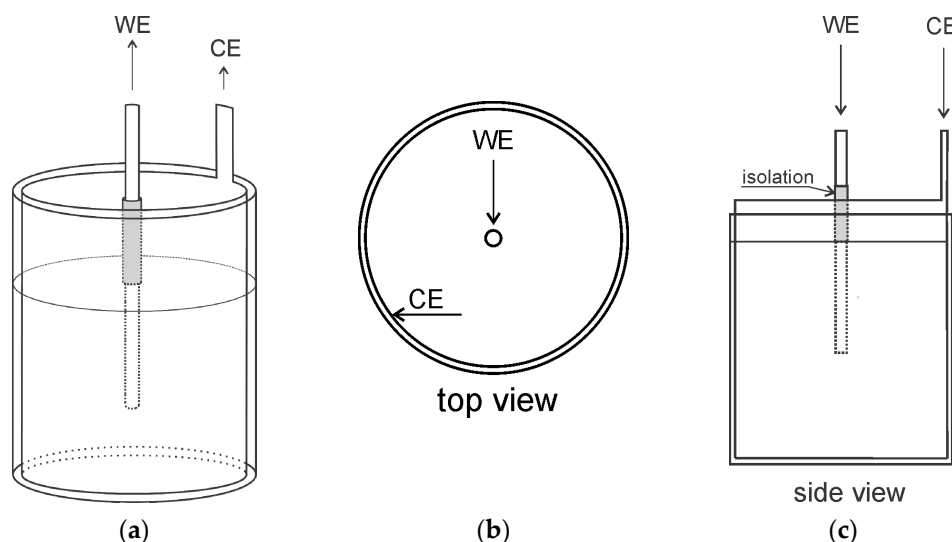**Figure 1.** (**a**) Scheme of the cell used for production of the Cu powders by electrolysis. WE—working electrode; CE—counter electrode, (**b**) top view, (**c**) side view.

The electrolytically produced powder was compared to the commercially supplied powder, Sigma-Aldrich company (Saint Louis, MO, USA), product No. 326453 (powder (spheroidal), 14–25 μm, 99%). Hereinafter, this powder is denoted as Cu(CHEM).

A scanning electron microscope (SEM)—TESCAN Digital Microscopy company (model VEGA3, Brno, Czech Republic) was used for the morphological characterization of the produced particles.

The Rigaku Ultima IV diffractometer (Rigaku Co. Ltd., Tokyo, Japan) with CuK$_\alpha$ radiation was used to study the crystal structure of the produced powders. Four reflections in the 2θ range between 30° and 95° were recorded in order to determine the preferred orientation of powder particles. For this purpose, calculation of the Texture Coefficient, *TC*(*hkl*) and Relative Texture Coefficient, *RTC*(*hkl*), based on an analysis of data obtained by the X-ray diffraction (XRD) method, was made. It was made in the following way: using an intensity of each reflection (*hkl*) plane, the following ratios (in percentage) were calculated by applying Equation (1) [35]:

$$R(hkl) = \frac{I(hkl)}{\sum\limits_{i}^{4} I(h_i k_i l_i)} \times 100 \qquad (1)$$

where *I*(*hkl*) is the intensity of each (*hkl*) reflection plane, while $\sum\limits_{i}^{4} I(h_i k_i l_i)$ represents the sum of intensities of all recorded reflection planes. Note: the values of intensities are given in cps.

Then, using the determined *R*(*hkl*) coefficients, the values of the Texture Coefficient, *TC*(*hkl*), were calculated by applying Equation (2):

$$TC(hkl) = \frac{R(hkl)}{R_s(hkl)} \qquad (2)$$

where $R_s(hkl)$ is determined in the same way as presented in Equation (1), but taking into consideration the Cu standard (04-0836).

In this way, accurate quantitative information about the absolute intensity of each of these reflections were obtained determining the $TC(hkl)$ coefficients. Also, the intensity of each reflection plane in relation to the other reflection planes represents the relevant information, and is defined as the Relative Texture Coefficient, $RTC(hkl)$ according to Equation (3):

$$RTC(hkl) = \frac{TC(hkl)}{\sum\limits_{i}^{4} TC(h_ik_il_i)} \times 100 \tag{3}$$

The $RTC(hkl)$ coefficient defines the intensity of the considered (hkl) orientation in relation to the standard which is included in the TC values.

A MALVERN Instruments MASTERSIZER 2000 (MALVERN Instruments Ltd., Malvern, Worcestershire, UK) device was used to determine the particle size distribution (PSD) and specific surface area (SSA) of the powders. Malvern Software (Version 5.60, MALVERN Instruments Ltd., Malvern, Worcestershire, UK) was used in order to obtain the SSA values.

Determination of the Average Current Efficiency of Hydrogen Evolution ($\eta_{I,av}(H_2)$)

In order to quantify the amount of hydrogen, generated in the galvanostatic electrolysis, the average current efficiency of hydrogen evolution, $\eta_{I,av}(H_2)$ was determined. For that purpose, the working and counter electrodes of Cu were placed in a burette which was positioned so that the overall volume of evolved hydrogen in the galvanostatic electrolysis remained in it. The surface area of the Cu working electrode, placed in a burette, was 0.63 cm^2. The current efficiency of hydrogen evolution in time t_i, $\eta_{I,i}(H_2)$, in %, is given by Equation (4):

$$\eta_{I,i}(H_2) = \frac{V(H_2)}{\mu(H_2)S_0jt_i} 100 \tag{4}$$

where

$$\mu(H_2) = \frac{V}{nF} = \frac{24{,}120 \text{ cm}^3}{2 \times 26.8 \text{ Ah}} = 450 \frac{\text{cm}^3}{\text{Ah}} \tag{5}$$

and $V(H_2)$ is the volume of evolved hydrogen in time t_i, nF is the number of Faradays per mole of spent ions, V is the molar volume of gas at temperature of 21.0 °C (i.e., 24,120 cm^3), S_0 is the surface of working electrode, and j is the current density of electrolysis. The average values of current efficiency for the hydrogen evolution reaction, $\eta_{I,av}(H_2)$ are determined as $\eta_{I,av}(H_2) = (1/t)\int\limits_0^t \eta_{I,i}(H_2)dt$, where t is time of electrolysis.

3. Results

3.1. Morphological Analysis of Cu Powders Produced by the Electrolytic and Non-Electrolytic Methods

The polarization curve for the copper electrodeposition from 0.10 mol dm^{-3} CuSO$_4$ in 0.50 mol dm^{-3} H$_2$SO$_4$ is shown in Figure 2. The plateau of the limiting diffusion current density was in the range of overpotentials between 300 and 750 mV, with a limiting diffusion current density value (j_L) of 9.6 mA cm^{-2}. In the galvanostatic regime of electrolysis, Cu in the powder form is formed at current densities larger than the limiting diffusion current density [19].

Morphologies of the Cu particles, obtained at current densities corresponding to 1.5 (j = 14.4 mA·cm^{-2}) and 40 (j = 384 mA·cm^{-2}) times larger values than the limiting diffusion current density, are shown in Figures 3 and 4, respectively. Considering the fact that the hydrogen evolution as the second reaction in the Cu electrolysis, commences inside the limiting diffusion current density plateau, a strong difference in the amount of generated hydrogen at these current densities, with strong

consequences for the morphology, structure and decisive characteristics of the obtained powders, was expected. Accordingly, inspection of the presented microphotographs shows the strong effect of the applied current densities on the morphology of Cu powder particles.
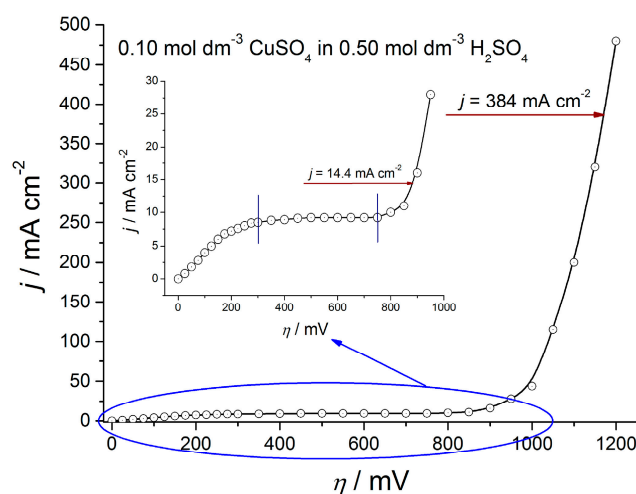

Figure 2. Polarization curve for the Cu electrodeposition from 0.10 mol·dm^{-3} CuSO$_4$ in 0.50 mol·dm^{-3} H$_2$SO$_4$.

Figure 3a shows the Cu deposit obtained immediately after finishing the process of electrolysis at 14.4 mA·cm^{-2}. The three morphological forms can be identified on this microphotograph: very branched 3D (three dimensional) dendritic forms, holes originating from detached hydrogen bubbles and cauliflower-like agglomerates of Cu grains. It can be seen that the shape of the dendritic forms (Figure 3a,b) was different from all of the so far observed forms of Cu dendrites. In previously observed forms of Cu dendrites, the tips of both the trunk and branches were sharp, while in this form they end with globules (Figure 3c,d). This form is observed for the first time in this investigation, and for this reason, it can be said that this shape represents a completely novel type of Cu dendrites. The size of the globules was from 3–5 μm for those in the branches, to about 10 μm at the tops of both branches and trunk. The size of the holes formed from the detached hydrogen bubbles, approached 100 μm. The typical cauliflower-like agglomerate of Cu grains, formed between the dendrites and holes is shown in Figure 3e. It consists of small agglomerates of Cu grains, surrounded by irregular channels. The size of the individual grains in these agglomerates was considerably smaller than the size of globules, and it was about 1 μm. The particles, obtained after removing the deposit from the electrode surface, are shown in Figure 3f,g. From a macromorphological point of view, no difference is observed between those on the electrode surface after the finished process of electrolysis and those after their removal. It is necessary to note the existence of channel structure inside the cauliflower-like particles (Figure 3f), which is a result of hydrogen evolution reaction.
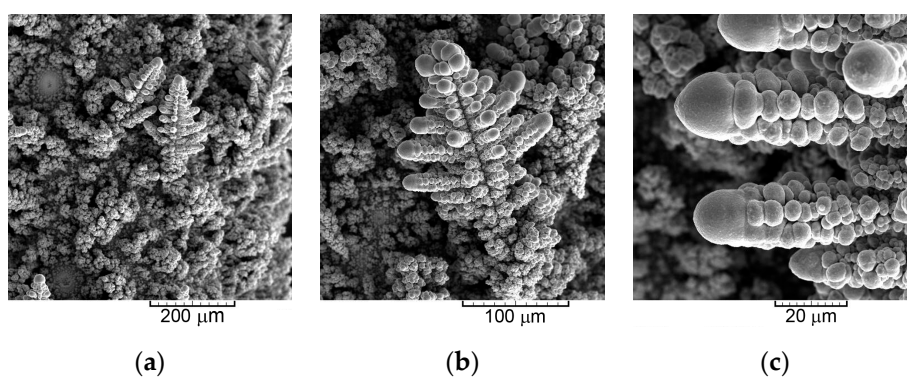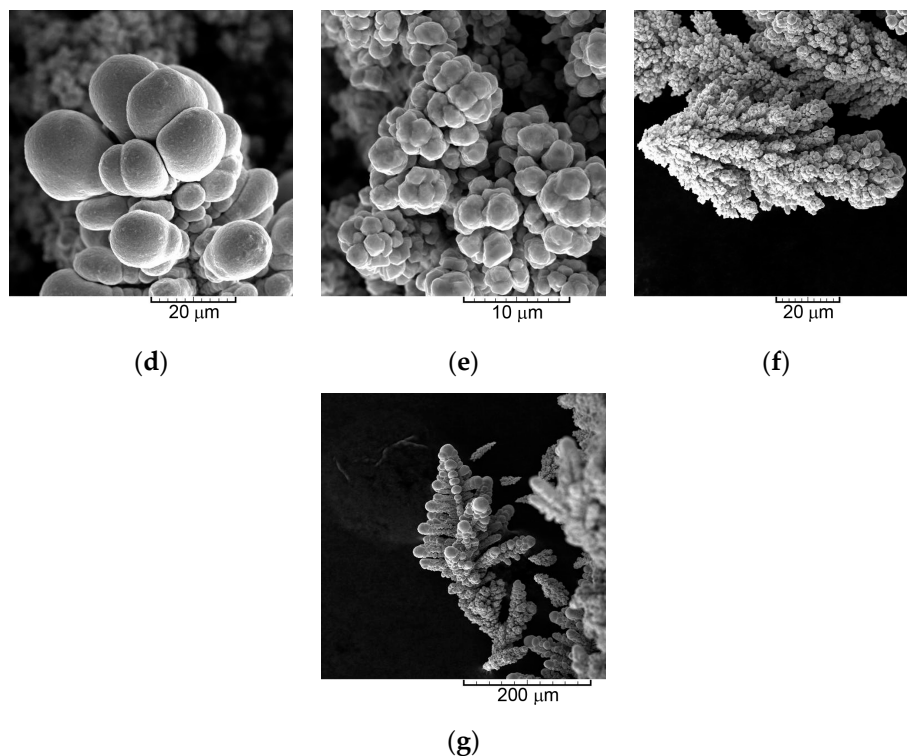

(**a**)　　　　　　　　　　　　(**b**)　　　　　　　　　　　　(**c**)

Figure 3. *Cont.*

Figure 3. Morphologies of the powdered copper obtained at a current density of 14.4 mA·cm^{-2}: (**a**) appearance of electrode surface after the process of electrolysis, (**b**) dendrite, (**c**) tops of branches of dendrite, (**d**) top of trunk of dendrite, (**e**) cauliflower-like agglomerates of Cu grains formed among dendrites and holes, (**f**,**g**) particles obtained after removal from the electrode surface.

Figure 4a shows the SEM microphotograph of copper electrode, obtained at a current density of 384 mA·cm^{-2}. A typical honeycomb-like structure, constructed from holes formed from the detached hydrogen bubbles (Figure 4b) surrounded by the disperse cauliflower-like agglomerates of Cu grains (Figure 4c,d) was obtained. Increasing the current density from 14.4 to 384 mA·cm^{-2} led to an intensification of the hydrogen evolution reaction, which is manifest by the increase in the number of holes and by a decrease in their size. In this case, a hole size was about 70 μm. As a result of intensification of the hydrogen evolution, the cauliflower-like agglomerates of Cu grains were more disperse than those obtained at 14.4 mA·cm^{-2}. The size of the grains in these agglomerates was about 200 nm, that is, approximately five times smaller than those formed at 14.4 mA·cm^{-2}. The typical forms of Cu particles, obtained by removal of deposit from the electrode surface, are shown in Figure 4e,f. Inhibition of dendritic growth and the cauliflower-like character of the formed particles as a result of vigorous hydrogen evolution, are clearly visible in Figure 4e,f.
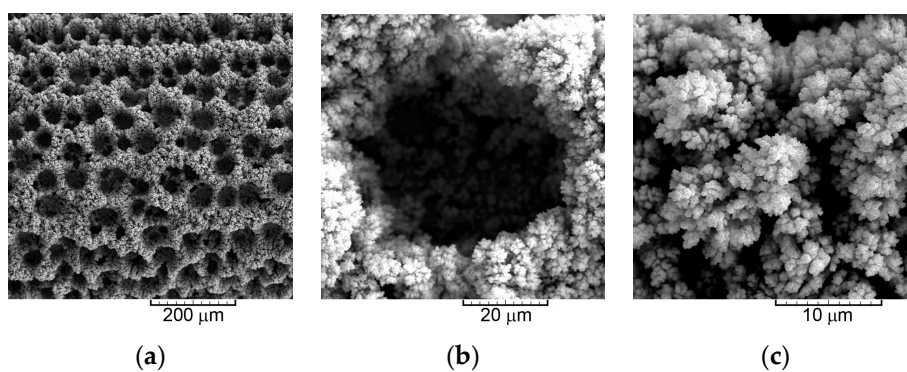

Figure 4. *Cont.*
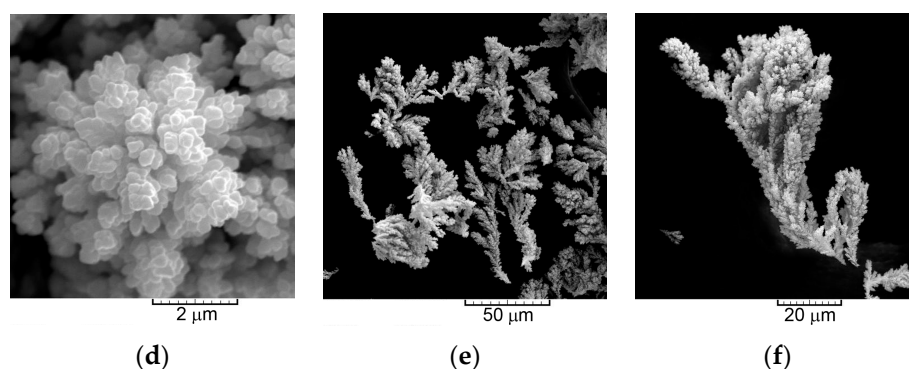
Figure 4. Morphologies of the powdered copper obtained at a current density of 384 mA·cm^{-2}:
(**a**) appearance of the electrode surface after the process of electrolysis (honeycomb-like structure),
(**b**) hole formed from the detached hydrogen bubble, (**c**) disperse cauliflower-like agglomerates
of Cu grains formed around holes, (**d**) typical agglomerate constructing disperse cauliflower-like
agglomerates, (**e**,**f**) particles obtained after removal from the electrode surface.

Figure 5 shows the morphology of commercially supplied Cu powder. It can be seen in Figure 5
that this powder consists of agglomerates of approximately spherical (spheroidal) grains of various
size. It can be seen that these agglomerates have a relatively compact structure. The size of these
agglomerates was larger than 10 μm, and they were constructed from grain sized in the range of
1–10 μm. Also, some of them had very irregular shapes. Considering the fact that these forms have
never been observed among electrolytically synthesized particles, it is clear that they are obtained in
some non-electrochemical way. The irregular, relatively compact forms constructed from approximately
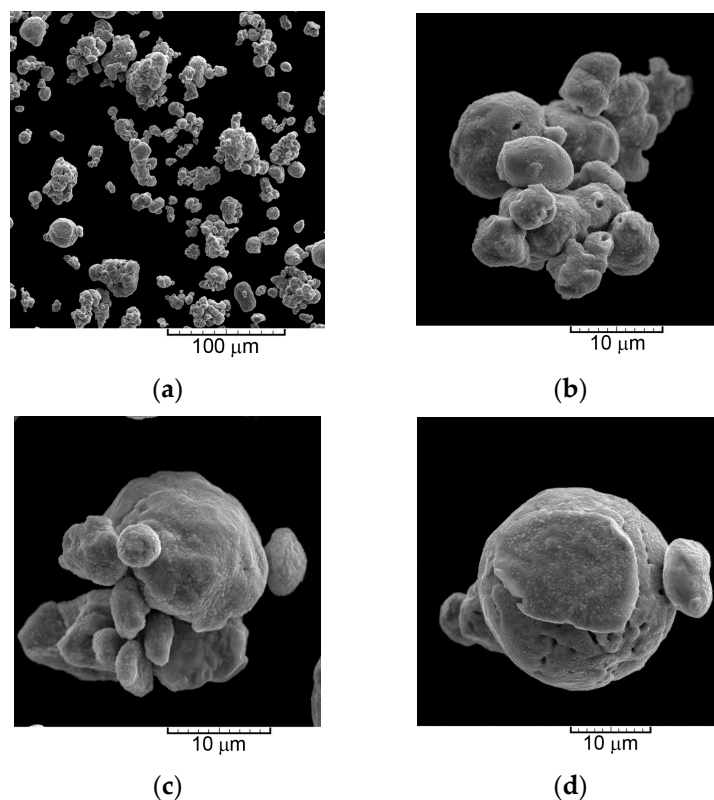spherical grains in a wide range of sizes confirmed this assumption.

Figure 5. Typical copper particles obtained by chemical processes: (**a**) ×500, (**b**) ×4000, (**c**) ×4500,
(**d**) ×3500.

3.2. Structural Analysis of Cu Powders Produced by the Electrolytic and Non-Electrolytic Methods

The XRD patterns of particles, obtained by removal the deposits obtained at current densities of 14.4 and 384 mA·cm^{-2}, and Cu standard (04-0836), are shown in Figure 6. The peaks at 2θ angles of 43.3°, 50.4°, 74.1° and 89.9° correspond to (111), (200), (220) and (311) crystal planes. The appearance of peaks at these angles confirms a face centered cubic (FCC) crystal lattice of Cu. A larger ratio of Cu crystallites oriented in the (111) plane observed in the both diffractograms, can be ascribed to the lower surface energy of this plane in relation to the other planes, because the surface energy (γ) values follow a trend: $\gamma_{111} < \gamma_{100} < \gamma_{110}$ [36,37]. The preferred orientation of the obtained particles was investigated by an analysis of the peak intensity ratios (111)/(200), (111)/(220) and (111)/(311), and by determination the $TC(hkl)$ and $RTC(hkl)$ coefficients.
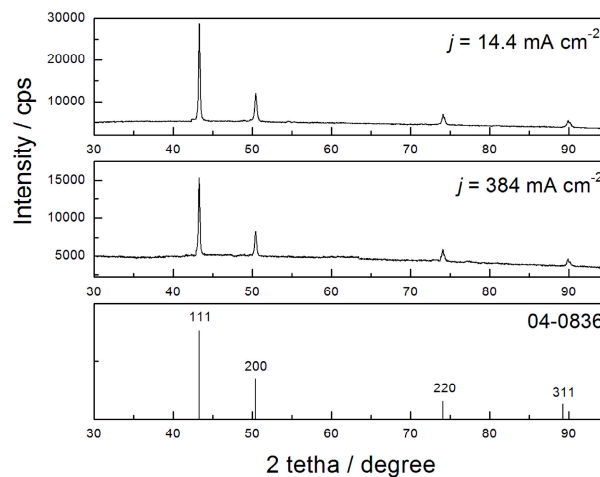

Figure 6. XRD patterns of Cu particles obtained at current densities of 14.4 and 384 mA·cm^{-2}, and Cu standard (04-0836).

The values of peak intensity ratios for the Cu particles produced at current densities of 14.4 mA·cm^{-2} (Cu(14.4)) and 384 mA·cm^{-2} (Cu(384)), and the same ratios for Cu standard are given in Table 1. It can be seen that (111)/(220) and (111)/(311) for the Cu(384) powder are considerably smaller than those for the Cu standard. On the other hand, for the Cu(14.4) powder, these ratios are still relatively close to the values for the Cu standard, indicating the random orientation of Cu crystallites in the particles shown in Figure 3. It is known [33] that the values of ratios considerably larger than those of the standard indicate the presence of (111) preferred orientation. However, there is no data about what happens with the crystal orientation when the peak intensity ratios are smaller than those of the standard. Therefore, the additional analysis of the crystal orientation of particles was carried out by determining the Texture Coefficient, $TC(hkl)$, and Relative Texture Coefficient, $RTC(hkl)$.

Table 1. Ratios of intensities of the diffraction peaks for the analyzed powders and Cu standard.

Type	Ratio of Intensities:		
of Powder Particles	(111)/(200)	(111)/(220)	(111)/(311)
Cu(14.4)	2.4	4.1	5.3
Cu(384)	1.9	2.6	3.4
Cu(CHEM)	2.5	5.2	6.0
Cu standard (04-0783)	2.2	5.0	5.9

The values of $TC(hkl)$ and $RTC(hkl)$ coefficients obtained for the electrolytically produced particles at current densities of 14.4 and 384 mA·cm^{-2} (Cu(14.4) and Cu(384), respectively) are given in Table 2. The values of $TC(hkl)$ coefficients larger than 1 indicate the existence of preferred orientation [33–35].

On the other hand, since four main reflections were analyzed, the values of *RTC* coefficients larger than 25% indicate the existence of a preferred orientation.

Table 2. Texture calculations for Cu powders obtained by the galvanostatic regime at current densities (*j*) of 14.4 and 384 mA·cm^{-2} and for commercially available powder (*j* = 14.4 mA·cm^{-2}—14.4, *j* = 384 mA·cm^{-2}—384, commercially available powder—CHEM, s—Cu standard).

Plane (*hkl*)	*R* (in %)			R_s (in %)	*TC*			*RTC* (in %)		
	$R_{14.4}$	R_{384}	R_{CHEM}		$TC_{14.4}$	TC_{384}	TC_{CHEM}	$RTC_{14.4}$	RTC_{384}	RTC_{CHEM}
(111)	54.1	45.3	57.3	54.6	0.99	0.83	1.05	23.6	17.3	26.6
(200)	22.5	24.1	22.3	25.1	0.90	0.96	0.89	21.5	20.0	22.5
(220)	13.1	17.2	10.9	10.9	1.20	1.58	1.00	28.6	32.9	25.3
(311)	10.3	13.4	9.5	9.4	1.10	1.43	1.01	26.3	29.8	25.6

The data analysis, presented in Table 2, shows that the values of the *RTC* coefficients for Cu(14.4) powder are about 25%, confirming the randomly orientated crystallites in the particles obtained at a current density of 14.4 mA·cm^{-2}. However, a different situation is observed when the particles produced at 384 mA·cm^{-2} were analyzed. The *RTC* coefficients for (220) and (311) planes are larger than those for the Cu standard, indicating the existence of a preferred orientation in these planes. Thus, it is clear that peak intensity ratios smaller than the values for the Cu standard (Table 1) indicate the preferred orientation in that plane.

Figure 7 shows the XRD pattern of chemically synthesized Cu powder (Cu(CHEM)) and Cu standard. The appearance of peaks at the same angles, as in the case of electrolytically produced Cu powders, confirms the face centered cubic (FCC) crystal lattice of Cu. Also, similar to the electrolytically produced powders, the Cu crystallites were predominately oriented in the (111) plane. The peak intensity ratios (111)/(200), (111)/(220) and (111)/(311) for this powder are included in Table 1. It can be seen in Table 1 that the values are very close to those for the Cu standard, confirming that the powder consists of randomly distributed spherical grains.
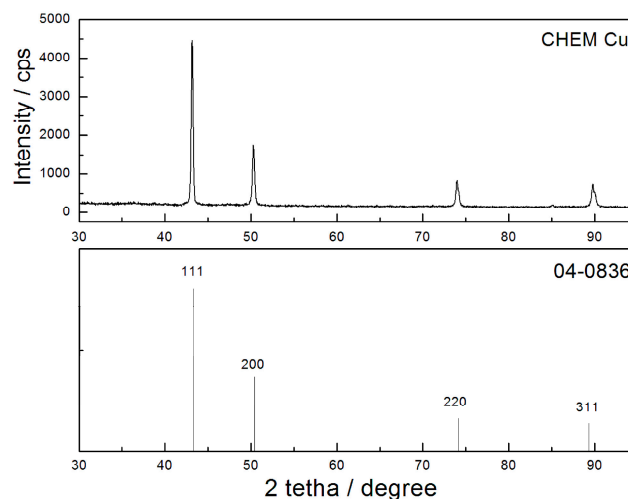

Figure 7. XRD pattern of chemically synthesized Cu powder, and Cu standard (04-0836).

The values of *TC*(*hkl*) and *RTC*(*hkl*) coefficients for this powder are shown in Table 2. The values of *TC* coefficients very close to 1, and *RTC* coefficients about 25%, clearly point to the random orientation of the Cu crystallites in these particles.

3.3. Analysis of the Specific Surface Area (SSA) and Particle Size Distribution (PSD) of the Considered Powders

To compare the powders obtained by the different methods of synthesis and under different conditions of electrolysis, the specific surface area (SSA) and particle size distribution (PSD), as two very important characteristics that describe the behavior of powders as a collection of the particles were analyzed. The values of the SSA for the analyzed powders are summarized in Table 3. It can be seen that the largest SSA value is obtained for the powder that consisted of disperse cauliflower-like particles obtained by electrolysis at 384 mA·cm^{-2}. The SSA of powder consisting of particles produced at this current density, was almost two time larger than the value for chemically synthesized powder. The smallest SSA value was obtained for the powder including the ordered dendritic structure galvanostatically produced at 14.4 mA·cm^{-2}.

Table 3. Values of specific surface area (SSA), particle size with the maximum volume ratio (PSMVR), and the average current efficiency for hydrogen evolution reaction ($\eta_{I,av}(H_2)$) for powders obtained by electrolysis at current densities of 14.4 mA·cm^{-2} (Cu(14.4)) and 384 mA·cm^{-2} (Cu(384)), and chemically synthesized powder (Cu(CHEM)).

The Type of Powder Particle	$\eta_{I,av}(H_2)$ %	SSA m^2 g^{-1}	PSMVR μm
Cu(14.4)	6.63	0.0389	23.2
Cu(384)	49.7	0.0997	10.9
Cu(CHEM)	/	0.0544	14.6

The PSD curves obtained for all three types of particles are shown in Figure 8. A uniform distribution of particles was obtained in all cases. The maximum volume ratios shift towards the smaller particle size in the same way as the increase of SSA. The maximum volume ratio for the powder produced at 384 mA·cm^{-2} corresponds to a particle size of 10.9 μm (this value as well as those obtained for the other powders are included in Table 3), and it is more than 50% smaller than the maximum volume ratio obtained at a current density of 14.4 mA·cm^{-2}, corresponding to a particle size of 23.2 μm. The presence of larger particles in powder produced at 384 mA·cm^{-2} (Figure 4e) is also identified in the PSD curve for this powder. For the chemically synthesized powder, the maximum volume ratio corresponds to a particle size of 14.6 μm, and it is situated between those for the electrolytically produced powders.

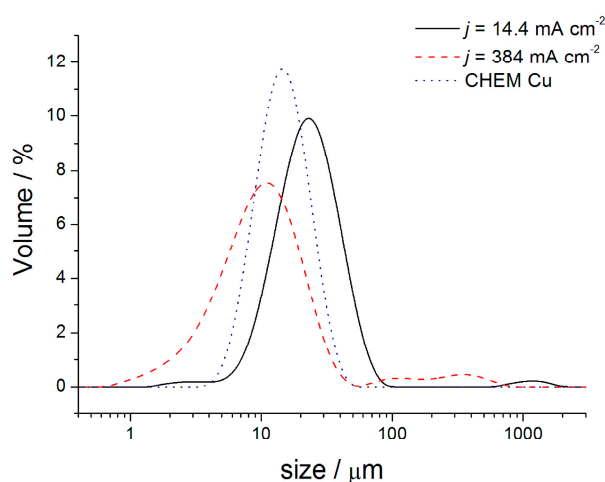**Figure 8.** Particle size distribution (PSD) curves obtained for the particles produced at current densities of 14.4 and 384 mA·cm^{-2}, and chemically synthesized powder.

4. Discussion

Three different morphologies of Cu particles were analyzed in this study: the 3D dendrites, disperse cauliflower-like agglomerates of Cu grains and compact agglomerates of Cu grains. Two of these were obtained by the electrolysis processes: 3D dendrites and disperse cauliflower-like agglomerates of Cu grains. Hydrogen evolution, as a parallel reaction to the Cu electrolysis at high current densities and overpotentials, had a crucial role in creating the final morphology of these particles. The amount of produced hydrogen is quantified by determination of the average current efficiency for hydrogen evolution, as presented in Figure 9 for the Cu electrolysis at current densities of 14.4 and 384 mA·cm^{-2}.

Figure 9 shows the dependencies of the evolved hydrogen volume and current efficiency for the hydrogen evolution reaction in a time t_i on the electrolysis time obtained at current densities of 14.4 (Figure 9a) and 384 mA·cm^{-2} (Figure 9b). It is clear that increasing the current density leads to a strong intensification in hydrogen evolution. The values of the average current efficiency for the hydrogen evolution reaction, obtained at the current densities of 14.4 and 384 mA·cm^{-2}, are given in Table 3.
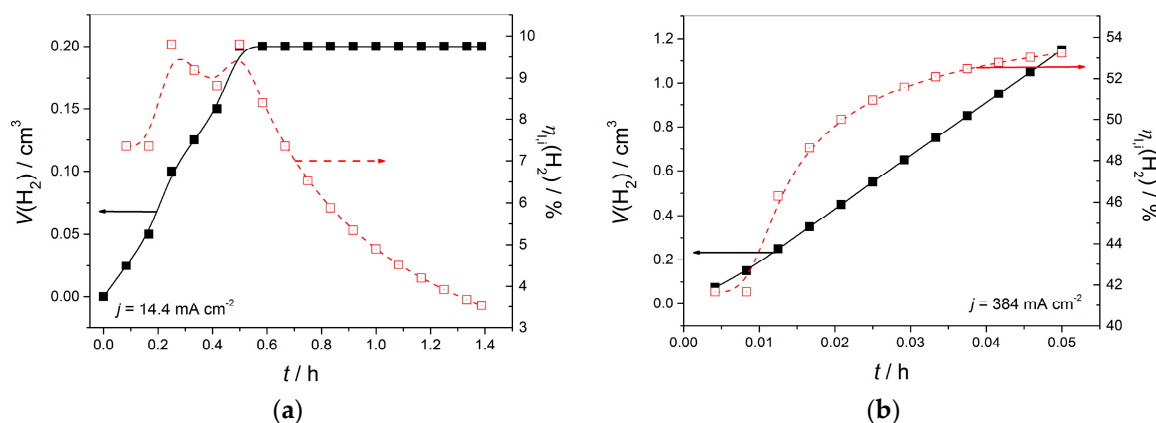

Figure 9. The dependencies of the evolved hydrogen volume and current efficiency for the hydrogen evolution reaction on the electrolysis time obtained at current densities of: (**a**) 14.4 mA·cm^{-2} and (**b**) 384 mA·cm^{-2}.

The amount of hydrogen that evolved at a current density of 14.4 mA·cm^{-2} was not sufficient to have any effect on the hydrodynamic conditions in the near-electrode layer. The proof for this is the rare holes formed from detached hydrogen bubbles and a somewhat non-uniform electrode surface determined by very branched 3D dendrites and cauliflower-like agglomerates of Cu grains (Figure 3a,b). As already mentioned, the 3D dendrites shown here represent a novel type of dendrite observed for the first time in this investigation. Formation of this type of dendrites can be explained from an electrochemical point of view in the following way: decrease of potential occurs with the electrolysis time in the galvanostatic regime of electrolysis. In this case, the potential at the end of electrolysis processes, corresponding to an amount passed electricity of 10 mA·h·cm^{-2}, was about 275 mV. This potential corresponds to the mixed activation-diffusion control at which formation of globules like those shown in Figure 3 occurs [19,38].

On the other hand, a very uniform honeycomb-like structure was formed at a current density of 384 mA·cm^{-2} (Figure 4). The amount of evolved hydrogen at this current density was vigorous enough to have a strong effect on the hydrodynamic conditions in the near-electrode layer. Namely, hydrogen generated during electrolysis causes a strong stirring of electrolyte in the near-electrode layer, leading to a decrease in diffusion layer thickness, an increase in the limiting diffusion current density, and a decrease in the degree of diffusion control in the electrodeposition process. The mechanism for the formation of the very disperse cauliflower-like particles, shown in Figure 4, was completely different to the one responsible for the formation of the dendritic particles (Figure 3). The concept

of "effective overpotential" can be applied to the formation of this particle type [19,39]. According to this concept, when hydrogen evolution is vigorous enough, the electrodeposition process occurs at an overpotential that is effectively lower than the specified one, and this overpotential is denoted as "effective" in the deposition process. From the morphological point of view, this means that the morphologies of metal deposits become similar to those obtained at some lower overpotentials at which the hydrogen evolution does not occur or is very slow. Formation of the cauliflower-like particles instead of dendrites confirms that there is a lower degree of diffusion control at this current density than at 14.4 mA·cm^{-2}.

The third type of particles are irregular compact agglomerates of Cu grains (Figure 5). On the basis of the macromorphology, which is determined by the compact irregular shapes, it is clear that the particles were formed by some non-electrochemical method of synthesis.

The XRD analysis showed that the chemically obtained particles and those obtained by electrolysis at 14.4 mA·cm^{-2} were randomly oriented. Unlike these, the electrolytically obtained particles at 384 mA·cm^{-2} showed (220) and (311) preferred orientation. The different preferred orientation of the particles produced by the galvanostatic regime of electrolysis can be explained from the electrochemical point of view using the basic laws related to the metal electrocrystallization processes [19]. Namely, the (111) plane is a "slow-growing" one, while the other planes ((200), (220) and (311)) are the "fast-growing" planes [33,40]. In the growth process, the "fast-growing" planes disappear, while the "slow-growing" (111) plane survives. This explains the predominant orientation of Cu crystallites in the (111) plane in particles obtained at both current densities. On the other hand, a nucleation rate depends on the potential according to Equation (6) [19]:

$$ J = K_1 \exp\left(-\frac{K_2}{E^2}\right) \tag{6} $$

where J is the nucleation rate, K_1 and K_2 are the constants independent of potential, and E is the potential. According to Equation (6), the nucleation rate increases with increasing the potential of electrolysis. At current density of 14.4 mA·cm^{-2}, a potential response was in the (275–900) mV range, while at 384 mA·cm^{-2}, this response was in the (1100–1250) mV range. Therefore, the nucleation rate was considerably larger at 384 mA·cm^{-2} than at 14.4 mA·cm^{-2}, causing the formation of a larger number of nuclei in the initial stage of electrolysis at 384 mA·cm^{-2} than at 14.4 mA·cm^{-2}. With the increased number of initially formed nuclei, there is an increased probability that the larger number of the "fast-growing" planes survive the growth process. In this way, the larger number of Cu crystallites oriented in (220) and (311) planes in the particles produced at 384 mA·cm^{-2} than at 14.4 mA·cm^{-2} can be explained.

The correlation between the morphology of the particles and crystal structure is also observed for some types of chemically synthesized particles. Namely, Cu nanowires synthesized under hydrothermal conditions using oleyl amine (OLA) and glucose as a reducing agent showed an XRD pattern with a higher intensity (200) peak than (111) peak [41]. The larger ratio of Cu crystallites oriented in the (200) plane than in (111) plane can be ascribed to the existence of a nanocubic structure [42], where a relatively large number of nanocubes coexist with the nanowires synthesized using OLA.

It is clear from the above consideration that electrolysis processes have certain advantages in the metal powder production over other methods. The advantages of this method include the easy control of the shape and size of particles by the choice of parameters of electrolysis. On the other hand, the particles obtained by chemical processes show a tendency towards aggregation [43], as observed here, which is avoided in the electrolysis processes by a vigorous hydrogen evolution reaction that can prevent this process. It is clear that the "current of hydrogen" formed through the interior of cauliflower-like particles (Figure 4e,f) prevents this aggregation.

5. Conclusions

Three types of particles with completely different shapes were analyzed by SEM, XRD and PSD. Two of them were obtained by electrolysis: the 3D dendrites and very disperse cauliflower-like agglomerates of the Cu grains. The third type of particle is a commercially available powder consisting of relatively compact agglomerates of the Cu grains. On the basis of the shape of particles, it was concluded that these particles were obtained by some non-electrochemical method.

Copper powders were synthesized by the galvanostatic regime of electrolysis at current densities of 14.4 and 384 mA·cm^{-2} at a temperature of 21.0 $\pm$ 0.5 °C using 0.10 mol·dm^{-3} CuSO$_4$ in 0.50 mol·dm^{-3} H$_2$SO$_4$. These current densities were selected to enable formation of either dendritic or cauliflower-like particles.

The dendrites obtained in this investigation ended in globules, which is different to the usual shape of Cu dendrites which have sharp tips at the top of the trunk and branches. The formation of globules at the tops of both the trunk and branches indicated the formation of a novel type of the Cu dendrites.

The Cu crystallites in the particles were randomly oriented (in both the electrolytic-produced powder at the current density of 14.4 mA·cm^{-2} and chemically synthesized powder) or showed (220) and (311) random orientation (in the galvanostatically produced powder at 384 mA·cm^{-2}). The change in preferred orientation for the galvanostatically produced powder was discussed on the basis of the theory of metal electrocrystallization.

The specific surface area of the Cu powders increased in the following order: SSA(14.4) < SSA(CHEM) < SSA(384).The particle size corresponding to the maximum volume ratio decreased similarly.

On the basis of comprehensive analysis of the three various forms of Cu powder particles, it is concluded that the powder obtained by electrolysis at the current density of 384 mA·cm^{-2} is more advantageous owing to it having the largest SSA and smallest particle size.

References

1. Copper and Copper Alloy Powder Metallurgy Properties and Applications. Available online: https://www.copper.org/resources/properties/129_6 (accessed on 13 November 2018).
2. Stopić, S.; Dvorak, P.; Friedrich, B. Synthesis of spherical nanosized copper powder by ultrasonic spray pyrolysis. *World Metall.* **2005**, *58*, 195–201.
3. Meshram, P.; Sinha, M.K.; Sahu, S.K.; Khan, P.; Pandey, B.D.; Mankhand, T.R. Solvothermal synthesis of high value copper powder from copper bleed solution of an indian copper smelter. *Powder Technol.* **2013**, *233*, 335–340. [CrossRef]
4. Jhajharia, R.; Jain, D.; Sengar, A.; Goyal, A.; Soni, P.R. Synthesis of copper powder by mechanically activated cementation. *Powder Technol.* **2016**, *301*, 10–15. [CrossRef]
5. Wu, S. Preparation of Fine Copper Powder using ascorbic acid as reducing agent and its application in MLCC. *Mater. Lett.* **2007**, *61*, 1125–1129. [CrossRef]
6. Sinha, A.; Das, S.K.; Vijaya Kumar, T.V.; Rao, V.; Ramachandrarao, P. Synthesis of nanosized copper powder by an aqueous route. *J. Mater. Synth. Process.* **1999**, *7*, 373–377. [CrossRef]

7. Wu, S.P.; Meng, S.Y. Preparation of micron size copper powder with chemical reduction method. *Mater. Lett.* **2006**, *60*, 2438–2442. [CrossRef]

8. Wu, S.P.; Ding, X.H. Preparation of fine copper powder with chemical reduction method and its application in MLCC. *IEEE Trans. Compon. Packag. Technol.* **2007**, *30*, 434–438. [CrossRef]

9. Lee, S.; Lee, D.; Lee, S.-Y.; Cho, S.-S.; Uhm, S. Fabrication of nano-sized copper powders in liquid media via high-energy electrical explosion method: Use of high purity copper recovered from waste jelly-filled cable as raw material. *Mater. Test.* **2016**, *58*, 161–164. [CrossRef]

10. Neikov, O.; Naboychenko, S.; Mourachova, I.; Gopienko, V.; Frishberg, I.; Lotsko, D. Production of copper and copper alloy powders. In *Handbook of Non-Ferrous Metal Powders: Technologies and Applications*; Elsevier: Oxford, UK, 2009; Chapter 16; pp. 331–332.

11. Rosenband, V.; Gany, A. Preparation of nickel and copper submicrometer particles by pyrolysis of their formats. *J. Mater. Process. Technol.* **2004**, *153*, 1058–1061. [CrossRef]

12. Chokratanasombat, P.; Nisaratanaporn, E. Preparation of ultrafine copper powders with controllable size via polyol process with sodium hydroxide addition. *Eng. J.* **2012**, *16*, 39–46. [CrossRef]

13. Amit, S.; Sharma, B.P. Preparation of copper powder by glycerol process. *Mater. Res. Bull.* **2002**, *37*, 407–416. [CrossRef]

14. Chow, G.M.; Kurihara, L.K.; Kemner, K.M.; Schoen, E.; Elam, W.T.; Ervin, A.; Keller, S.; Zhang, Y.D.; Budnick, J.; Ambrose, T. Structural, morphological, and magnetic study of nanocrystalline cobalt-copper powders synthesized by the polyol process. *J. Mater. Res.* **1995**, *10*, 1546–1554. [CrossRef]

15. Djokić, S.S. Production of Metallic Powders from Aqueous Solutions without an External Current Source. In *Electrochemical Production of Metal Powders, Series: Modern Aspects of Electrochemistry*; Djokić, S.S., Ed.; Springer: New York, NY, USA, 2012; Volume 54, pp. 369–398.

16. Djokić, S.S.; Djokić, N.S. Electroless deposition of metallic powders. *J. Electrochem. Soc.* **2011**, *158*, D204–D209. [CrossRef]

17. Reverberi, A.P.; Salerno, M.; Lauciello, S.; Fabiano, B. Synthesis of copper nanoparticles in ethylene glycol by chemical reduction with vanadium (+2) salts. *Materials* **2016**, *9*, 809. [CrossRef] [PubMed]

18. Park, T.J.; Lee, K.G.; Lee, S.Y. Advances in microbial biosynthesis of metal nanoparticles. *Appl. Microbiol. Biotechnol.* **2016**, *100*, 521–534. [CrossRef] [PubMed]

19. Popov, K.I.; Djokić, S.S.; Nikolić, N.D.; Jović, V.D. *Morphology of Electrochemically and Chemically Deposited Metals*; Springer: New York, NY, USA, 2016; pp. 1–368.

20. Nikolić, N.D.; Pavlović, Lj.J.; Pavlović, M.G.; Popov, K.I. Morphologies of electrochemically formed copper powder particles and their dependence on the quantity of evolved hydrogen. *Powder Technol.* **2008**, *185*, 195–201. [CrossRef]

21. Orhan, G.; Hapci, G. Effect of electrolysis parameters on the morphologies of copper powder obtained in a rotating cylinder electrode cell. *Powder Technol.* **2010**, *201*, 57–63. [CrossRef]

22. Orhan, G.; Gezgin, G.G. Effect of electrolysis parameters on the morphologies of copper powder obtained at high current densities. *J. Serb. Chem. Soc.* **2012**, *77*, 651–665. [CrossRef]

23. Ostanina, T.N.; Rudoi, V.M.; Patrushev, A.V.; Darintseva, A.B.; Farlenkov, A.S. Modelling the dynamic growth of copper and zinc dendritic deposits under the galvanostatic electrolysis conditions. *J. Electroanal. Chem.* **2015**, *750*, 9–18. [CrossRef]

24. Nikolić, N.D.; Branković, G.; Pavlović, M.G. Correlate between morphology of powder particles obtained by the different regimes of electrolysis and the quantity of evolved hydrogen. *Powder Technol.* **2012**, *221*, 271–277. [CrossRef]

25. Nekouei, R.K.; Rashchi, F.; Joda, N.N. Effect of organic additives on synthesis of copper nano powders by pulsing electrolysis. *Powder Technol.* **2013**, *237*, 554–561. [CrossRef]

26. Popov, K.I.; Pavlović, Lj.J.; Ivanović, E.R.; Radmilović, V.; Pavlović, M.G. The effect of reversing current deposition on the apparent density of electrolytic copper powder. *J. Serb. Chem. Soc.* **2002**, *67*, 61–67. [CrossRef]

27. Pavlović, M.G.; Pavlović, Lj.J.; Maksimović, V.M.; Nikolić, N.D.; Popov, K.I. Characterization and morphology of copper powder particles as a function of different electrolytic regimes. *Int. J. Electrochem. Sci.* **2010**, *5*, 1862–1878.

28. Nekouei, R.K.; Rashchi, F.; Ravanbakhsh, A. Copper nanopowder synthesis by electrolysis method in nitrate and sulfate solutions. *Powder Technol.* **2013**, *250*, 91–96. [CrossRef]

29. Nekouei, R.K.; Rashchi, F.; Amadeh, A.A. Using design of experiments in synthesis of ultra-fine copper particles by electrolysis. *Powder Technol.* **2013**, *237*, 165–171. [CrossRef]

30. Lou, W.; Cai, W.; Li, P.; Su, J.; Zheng, S.; Zhang, Y.; Jin, W. Additives-assisted electrodeposition of fine spherical copper powder from sulfuric acid solution. *Powder Technol.* **2018**, *326*, 84–88. [CrossRef]

31. Bakthavatsalam, R.; Ghosh, S.; Biswas, R.K.; Saxena, A.; Raja, A.; Thotiyl, M.O.; Wadhai, S.; Banpurkar, A.G.; Kundu, J. Solution chemistry-based nano-structuring of copper dendrites for efficient use in catalysis and superhydrophobic surfaces. *RSC Adv.* **2016**, *6*, 8416–8430. [CrossRef]

32. Copper Powder. Available online: http://www.cnpcpowder.com/products/copper/ (accessed on 13 November 2018).

33. Avramović, Lj.; Pavlović, M.M.; Maksimović, V.M.; Vuković, M.; Stevanović, J.S.; Bugarin, M.; Nikolić, N.D. Comparative morphological and crystallographic analysis of electrochemically- and chemically-produced silver powder particles. *Metals* **2017**, *7*, 160. [CrossRef]

34. Avramović, Lj.; Ivanović, E.R.; Maksimović, V.M.; Pavlović, M.M.; Vuković, M.; Stevanović, J.S.; Nikolić, N.D. Correlation between crystal structure and morphology of potentiostatically electrodeposited silver dendritic nanostructures. *Trans. Nonferr. Met. Soc. China* **2018**, *28*, 1903–1912. [CrossRef]

35. Berube, L.P.; Esperance, G.L. A quantitative method of determining of the degree of texture of zinc electrodeposits. *J. Electrochem. Soc.* **1989**, *136*, 2314–2315. [CrossRef]

36. Sivasubramanian, R.; Sangaranarayanan, M.V. Electrodeposition of silver nanostructures: From polygons to dendrites. *CrystEngComm* **2013**, *15*, 2052–2056. [CrossRef]

37. Xia, Y.; Xiong, Y.; Lim, B.; Skrabalak, S.E. Shape-controlled synthesis of metal nanocrystals: Simple chemistry meets complex physics? *Angew. Chem. Int. Ed.* **2009**, *48*, 60–103. [CrossRef] [PubMed]

38. Popov, K.I.; Živković, P.M.; Jokić, B.; Nikolić, N.D. The shape of the polarization curve and diagnostic criteria for the metal electrodeposition process control. *J. Serb. Chem. Soc.* **2016**, *81*, 291–306. [CrossRef]

39. Nikolić, N.D.; Popov, K.I.; Pavlović, Lj.J.; Pavlović, M.G. The effect of hydrogen codeposition on the morphology of copper electrodeposits. I. The concept of effective overpotential. *J. Electroanal. Chem.* **2006**, *588*, 88–98. [CrossRef]

40. Nikolić, N.D.; Maksimović, V.M.; Branković, G. Morphological and crystallographic characteristics of electrodeposited lead from the concentrated electrolyte. *RSC Adv.* **2013**, *3*, 7466–7471. [CrossRef]

41. Ravi Kumar, D.V.; Kim, I.; Zhong, Z.; Kim, K.; Lee, D.; Moon, J. Cu(II)–alkyl amine complex mediated hydrothermal synthesis of Cu nanowires: Exploring the dual role of alkyl amines. *Phys. Chem. Chem. Phys.* **2014**, *16*, 22107–22115. [CrossRef] [PubMed]

42. Yang, H.-J.; He, S.-Y.; Chen, H.-L.; Tuan, H.-Y. Monodisperse copper nanocubes: Synthesis, self-assembly, and large-area dense-packed films. *Chem. Mater.* **2014**, *26*, 1785–1793. [CrossRef]

43. Lu, L.; Sevonkaev, I.; Kumar, A.; Goia, D.V. Strategies for tailoring the properties of chemically precipitated metal powders. *Powder Technol.* **2014**, *261*, 87–97. [CrossRef]